Additively manufactured electrodes for the electrochemical detection of hydroxychloroquine

Mayane S. Carvalho [a], Raquel G. Rocha [a], Lucas V. de Faria [a], Eduardo M. Richter [a,c], Luiza M.F. Dantas [b], Iranaldo S. da Silva [b,*], Rodrigo A.A. Muñoz [a,c,**]

[a] Institute of Chemistry, Federal University of Uberlândia, 38408-100, Uberlândia, MG, Brazil
[b] Chemistry Technology Department, Federal University of Maranhão, 65080-805, São Luis, Maranhão, Brazil
[c] National Institute of Science and Technology in Bioanalytics (INCT-Bio), Campinas, SP, Brazil

ARTICLE INFO

ABSTRACT

Although studies have demonstrated the inactivity of hydroxychloroquine (HCQ) towards SARS-CoV-2, this compound was one of the most prescribed by medical organizations for the treatment of hospitalized patients during the coronavirus pandemic. As a result of it, HCQ has been considered as a potential emerging contaminant in aquatic environments. In this context, we propose a complete electrochemical device comprising cell and working electrode fabricated by the additive manufacture (3D-printing) technology for HCQ monitoring. For this, a 3D-printed working electrode made of a conductive PLA containing carbon black assembled in a 3D-printed cell was associated with square wave voltammetry (SWV) for the fast and sensitive determination of HCQ. After a simple surface activation procedure, the proposed 3D-printed sensor showed a linear response towards HCQ detection (0.4–7.5 µmol L^{-1}) with a limit of detection of 0.04 µmol L^{-1} and precision of 2.4% (n = 10). The applicability of this device was shown to the analysis of pharmaceutical and water samples. Recovery values between 99 and 112% were achieved for tap water samples and, in addition, the obtained concentration values for pharmaceutical tablets agreed with the values obtained by spectrophotometry (UV region) at a 95% confidence level. The proposed device combined with portable instrumentation is promising for on-site HCQ detection.

1. Introduction

Hydroxychloroquine (HCQ), chemical structure shown in Fig. 1, is a compound derivative from chloroquine, which differs by the presence of a hydroxyl group [1,2]. It has been used as antimalarial and immuno-modulatory (systemic and cutaneous lupus erythematosus) drugs, as well as, applied for several rheumatic diseases because of its anti-inflammatory properties [3–7]. Moreover, HCQ has antiviral properties and because of it, some medical organizations had recommended its use in the treatment of severe acute respiratory syndrome coronavirus (SARS-CoV-2) [8–13]. However, serious adverse effects, such as hypoglycemia, cardiomyopathy, gastrointestinal toxicity and neurological reactions, have been reported when this drug is used in the treatment of infected patients with SARS-CoV-2 [11,14–17]. In fact, although prescribed, this compound does not confer protection against COVID-19 infection, as highlighted in some studies [18–20].

Considering its wide use during the pandemic scenario and that 25% of the compound is excreted as its unmetabolized form in the urine according to pharmacokinetic data [21], HCQ has been recognized as a potential emerging contaminant. Hence, it is essential to develop sensitive, rapid, and simple analytical methods for monitoring HCQ in pharmaceutical formulations and other matrices.

According to the literature, chromatographic and spectrophotometric methods are widely reported for HCQ determination [22–27]. Although these methods present accuracy and sensitivity, they require costly and bulky instrumentation, time-consuming analysis, and specialized professional. On the other hand, electrochemical methods have been employed for HCQ detection in different matrices using conventional electrodes, such as boron-doped diamond (BDD) and modified glassy carbon electrodes (GCE) [28–32]. In fact, these electroanalytical methods showed attractive sensing characteristics, however, BDD and modified GCE are not easily implemented for in-field
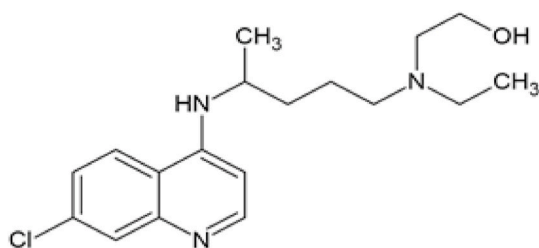

Fig. 1. Molecular structure of HCQ.

analyses because of their cost (cost-effective for large scale production) and surface modification requirements. In this sense, additive manufacturing, also known as 3D-printing, seems to be a promising technology for the development of electrochemical devices due to its characteristics, such as fast prototyping with large-scale production, low energetic demand, and accessible 3D printers, especially when using fused deposition modeling (FDM) models [33–35].

In FDM process, three-dimensional materials are constructed using thermoplastic filaments that are heated, extruded, and deposited layer-by-layer on a heated platform [36]. Commercially-available conductive filaments made of polylactic acid composites containing a conductive agent (Proto-Pasta® contains carbon-black (CB) and Black-Magic® contains graphene (Gr)) have enabled the production of electrochemical sensors with high performance in the detection of molecules of pharmaceutical, forensic and environmental interests [37–42]. João and coauthors [43] showed the detection of atropine in beverage samples, and Cardoso et al. [44] showed the detection of different molecules (catechol, dopamine) using 3D-printed Gr-PLA electrodes. Additionally, Cardoso and collaborators used the same 3D-printed electrochemical disposable for the detection of 2,4,6-trinitrotoluene (TNT) [45]. However, commercial filament composed by Gr-PLA presents higher cost when compared to CB-PLA filament [45]. In this sense, our group research demonstrated that the detection of TNT was also possible using 3D-printed CB-PLA electrodes with similar electroanalytical performance. Moreover, the detection of chloramphenicol [46], naproxen [47], antioxidants [48], sulfanilamide [49] uric acid and zinc [50], adrenaline [51], steroid hormones [40] and reduction of carbon dioxide [52] was also demonstrated with appropriate analytical performance. Herein, we demonstrated, for the first time, that 3D-printed CB-PLA electrodes can be applied for the determination of HCQ in pharmaceutical and tap water samples by square-wave voltammetry (SWV).

2. Experimental section

2.1. Reagents and samples

All reagents were of analytical grade and used without further purification. Hydroxychloroquine sulfate (98% w/w) and azithromycin (98% w/w) were purchased from Sigma Aldrich (Darmstadt, Germany). Paracetamol, Caffeine (99% w/w), ferricyanide potassium, and phosphoric acid (85% w/v) were obtained from Labsynth (São Paulo, Brazil). Potassium chloride (99.5% w/w) was purchased from Carlo Erba (Emmendingen, Germany). Ethanol (99.3% v/v) was obtained from Sciavicco (Minas Gerais, Brazil). Acetic acid (98% w/v) was purchased from Vetec (Rio de Janeiro, Brazil). The boric acid (99.8% w/w) and sodium hydroxide (98% w/w) were obtained from AppliChem Panreac (Barcelona, Spain). Acetylsalicylic acid was obtained from Essência (Uberlândia, Brazil). All aqueous solutions used were prepared daily, employing high purity deionized water with the resistivity at least 18 MΩ cm, purchased from a Milli Q water purification process (Millipore, Bedford, MA, USA).

Britton-Robinson (BR) buffer (0.12 mol L^{-1}) was used as the supporting electrolyte for all electrochemical measurements. This buffer was composed of a mixture of acetic, boric, and phosphoric acids, both
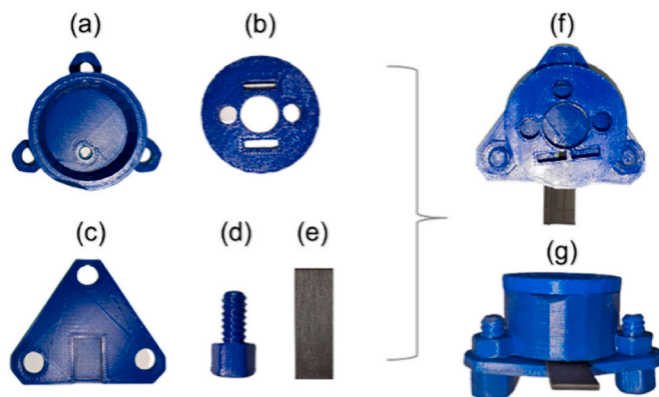

Fig. 2. Real images of components of the 3D-printed cell (top view): (a) body cell; (b) top cover; (c) bottom cover; (d) screw; (e) 3D-printed CB-PLA working electrode; (f and g) top and front views of assembled 3D-printed cell.

in 0.04 mol L^{-1}. A sodium hydroxide solution (1 mol L^{-1}) was used to adjust the pH values in the range from 2.0 to 10.0.

Stock solutions of HCQ (1.5 mmol L^{-1}) were freshly prepared to prevent photodegradation [53] by dissolution in deionized water and dilution in appropriate supporting electrolyte. Pharmaceutical samples (tablets) were obtained from local drug stores. Ten tablets from the same brand (400 mg per tablet) were powdered in a mortar/pestle and an amount of the power (~4 mg) was dissolved and diluted 2000-fold in the supporting electrolyte and immediately analyzed. Two tap water samples were collected using a plastic centrifuge tube and subsequently spiked with HCQ levels concentrations (10 and 15 µmol L^{-1}) respectively, followed by a dilution process (9-fold) in the supporting electrolyte.

2.2. Apparatus for electrochemical and spectrophotometric (UV–vis) measurements

Cyclic and square-wave voltammetric measurements were performed using a µ-AUTOLAB type III potentiostat/galvanostat (Metrohm Autolab BV, Utrecht, Netherlands). The acquisition and processing data were acquired using NOVA 2.1.4 software. All electrochemical measurements were performed at room temperature in the presence of dissolved oxygen. A platinum wire and a lab-made Ag|AgCl|KCl$_{(sat.)}$ were used as counter and reference electrodes, respectively. A spectrophotometer (FEMTO 600s, Brazil) equipped 1 cm quartz cell at 342 nm was used for UV measurements as described by Ferraz et al. [54].

2.3. Fabrication of 3D-printed CB-PLA electrode

A commercial filament composed by a mixture of CB and PLA (Protopasta, WA, USA) was used to construct of 3D-printed electrodes. A rectangular piece (38 mm length x 11 mm width) was printed employing Flashforge Dreamer NX printer and printing parameters described in Table S1. The faces of the model were used as working electrode, according to previous works [44,55]. A 3D-printed electrochemical cell (internal volume of 10 mL) was manufacture as described by Cardoso et al. [44]. Briefly, 3D-printed cell was produced using an acrylonitrile butadiene styrene (ABS, GTMax, São Paulo, Brazil). A real image of this cell is shown in Fig. 2. The parts of the cell include: (a) cell container; (b) top cover with two orifices to allocate counter and reference electrodes; (c) bottom part containing three holes for the insertion of (d) screws; (e) 3D-printed working electrode. Top (f) and (g) front of views of the 3D-printed cell. A rubber O-ring was allocated over the working electrode that limited the geometric electrode area (0.18 cm^2).

Before use, the rectangular face was polished with abrasive paper (3 M 1200 Grit) in deionized water and submitted to an electrochemical treatment, according to literature, which consisted of electrochemical
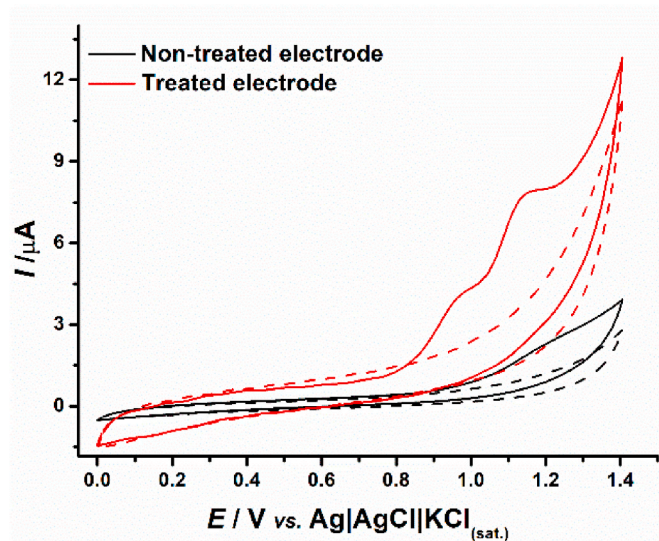
Fig. 3. Cyclic voltammetric profiles obtained for 28 μmol L^{-1} HCQ at the 3D-printed CB-PLA electrode before (black line) and after electrochemical treatment (red line), using 0.12 mol L^{-1} BR buffer (pH = 7.0). The dashed lines are the respective blanks. Voltammetric conditions: scan rate: 50 mV s^{-1}; step potential: 5 mV. (For interpretation of the references to colour in this figure legend, the reader is referred to the Web version of this article.)

activation using a 0.5 mol L^{-1} NaOH solution, applying +1.4 V (*vs.* Ag|AgCl|KCl$_{(sat.)}$) for 200 s followed by −1.0 V (*vs.* Ag|AgCl|KCl$_{(sat.)}$) for 200 s.

3. Results and discussion

3.1. Effect of the chemical/electrochemical surface treatment on the electrochemical oxidation of HCQ

Preliminary studies by cyclic voltammetry were carried out in order to investigate the influence of the electrode treatment on the HCQ electrochemical response. For this, cyclic voltammograms were recorded in the presence 28 μmol L^{-1} HCQ using the treated and non-treated electrodes and BR buffer (0.12 mol L^{-1}, pH = 7.0) as the supporting electrolyte (Fig. 3). As can be seen, a low-intensity oxidation process (at around +1.2 V *vs.* Ag|AgCl|KCl$_{(sat.)}$) was obtained using an untreated electrode (black line). In contrast, a better voltammetric profile was achieved at the treated 3D-printed CB-PLA surface (red line), where two well-defined oxidation signals were observed (at around +0.9 and + 1.2 V *vs.* Ag|AgCl|KCl$_{(sat.)}$). This last result is more consistent with other studies using carbon-based electrodes for HCQ detection [32,56]. As discussed in previous studies reported by our research group [38,57,58], the chemical/electrochemical treatment in an alkaline solution (0.5 mol L^{-1} NaOH) provides the consumption of the insulating material (PLA) via saponification reaction and exposes a greater amount of CB conductive sites, which contributes to increasing the electrode porosity and consequently the access to the conductive sites. Richter et al. [38] showed by microscopic techniques that the conductive sites become more available after the treatment . Moreover, XPS analyses showed
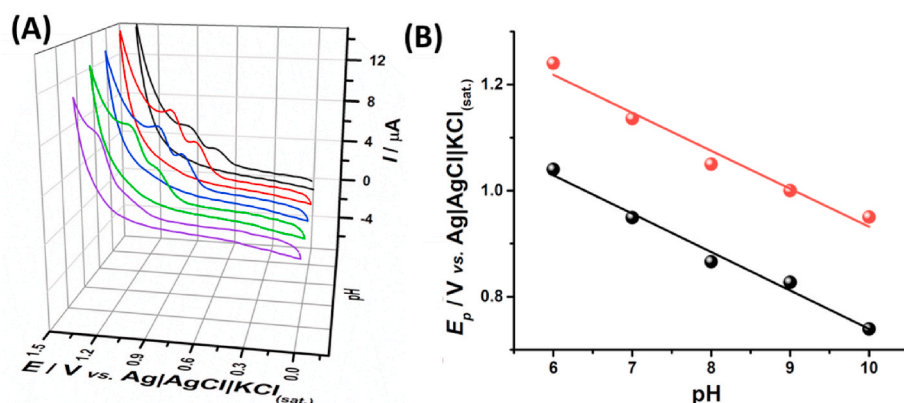

Fig. 4. (A) Cyclic voltammetric responses obtained for 28 μmol L^{-1} HCQ in 0.12 mol L^{-1} BR buffer of different pHs (purple line, pH = 6.0); (green line, pH = 7.0); (blue line, pH = 8.0); (red line; pH = 9.0); (black line, pH = 10.0). **(B)** Relation between pH and peak potential (E$_p$) for the first (black line) and second (red line) oxidation processes of HCQ. Voltammetric parameters: scan rate of 50 mV s^{-1} and step potential of 5 mV. (For interpretation of the references to colour in this figure legend, the reader is referred to the Web version of this article.)

Fig. 5. (A) Cyclic voltammetric responses obtained for 28 μmol L^{-1} HCQ in 0.12 mol L^{-1} BR buffer (pH = 9.0) varying scan rates (10–150 mV s^{-1}). (B) Relationship of the peak potential (Ep) as a function of the log ν for the first (black line) and second (red line) electrochemical processes. (For interpretation of the references to colour in this figure legend, the reader is referred to the Web version of this article.)
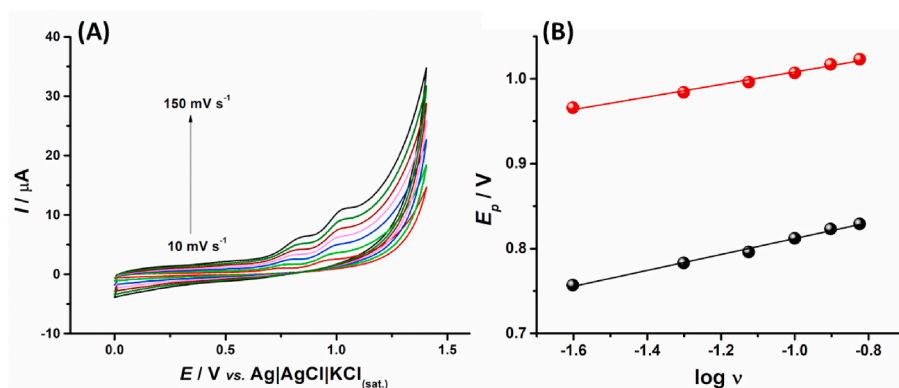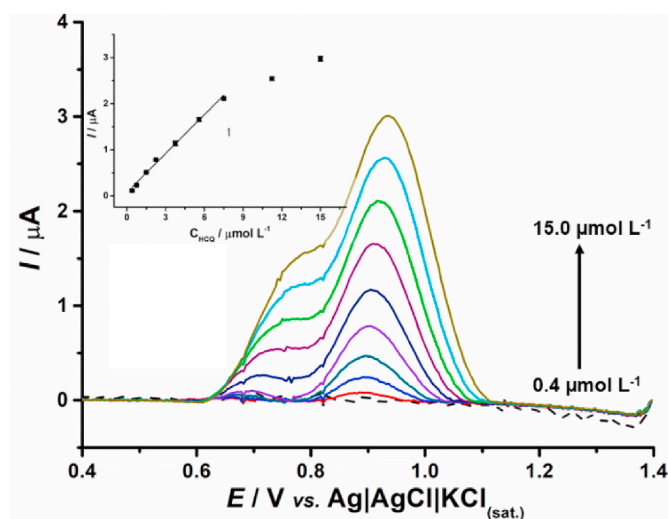
Fig. 6. Baseline-corrected SWV responses obtained for increasing concentrations (0.4–15 µmol L^{-1}) of HCQ using 0.12 mol L^{-1} BR buffer (pH = 9.0) at 3D-printed CB-PLA electrodes and respective calibration plot (inset in Fig. 4). SWV conditions: amplitude = 70 mV; step potential = 4 mV; frequency = 30 s^{-1}.

changes of carbon functional groups on the electrode surface that may explain the improvement of the electrochemical activity. In this sense, the treated 3D-printed CB-PLA electrode was selected for further studies.

The electrochemical behavior of HCQ was evaluated in BR buffer in pH values ranging from 6.0 to 10.0, as shown in Fig. 4. As noted, throughout the investigated pH range, HCQ exhibited two pH-dependent oxidation processes and the linear relationship between peak potential (E$_p$) and pH for both processes with slope values (70 and 71 mV for first and second oxidation processes, respectively) remarkably close to 59 mV pH^{-1} in which indicate equal number of electron and protons involved in these electrochemical processes (Fig. 4), as reported in the literature [2,29,31].

Considering that pH 9.0 provided a better electrochemical response (peak shape and peak height) and that the oxidation peak potential shifted to less positive values (HCQ can be detected at a lower potential), this pH was selected. Under this condition, the mass transport of electrochemical reactions of HCQ (28 µmol L^{-1}) was checked using scan rate (ν) from 10 to 150 mV s^{-1} (Fig. S1 and Fig. 5A). Linear relationship between peak current and scan rate (r$^2 \geq$ 0.99) for both oxidation processes indicated a mass transport regime controlled by the adsorption of HCQ species (Fig. S1). Such a behavior agrees with other studies involving carbon-based surfaces [7,59].

According to Laviron [60], the potential peak (E$_p$) is dependent with log ν for adsorption-controlled process, as described above (Eq. (1)):

$$E_p = A + \frac{2.303\,RT}{(1-\alpha)nF} \log \nu \tag{1}$$

Where *A* is a constant related to the formal electrode potential (E$_0$) and standard rate constant at (E$_0$), *n* is the number of electrodes involved in the reaction, *R* the universal constant of gases (8.314 J mol K^{-1}), *F* Faraday constant, *T* is temperature (298 K) and α is the coefficient of electron transfer. Therefore, using the Laviron equation and assuming a value of α = 0.5, as described for organic species with irreversible electrochemical processes, the transferred electron is calculated to be 1.2 and 1.6 for first and second processes, respectively (Fig. 5B). These values suggest that one and two electrons were involved in the first and second electrochemical processes, respectively. Our results agree with other works reported in the literature for the mechanism reaction of HCQ, in which the first and second oxidation processes occur in the aromatic amine and hydroxyl group of this molecule [2,30,61].

In next experiments, only the second oxidation process (at around
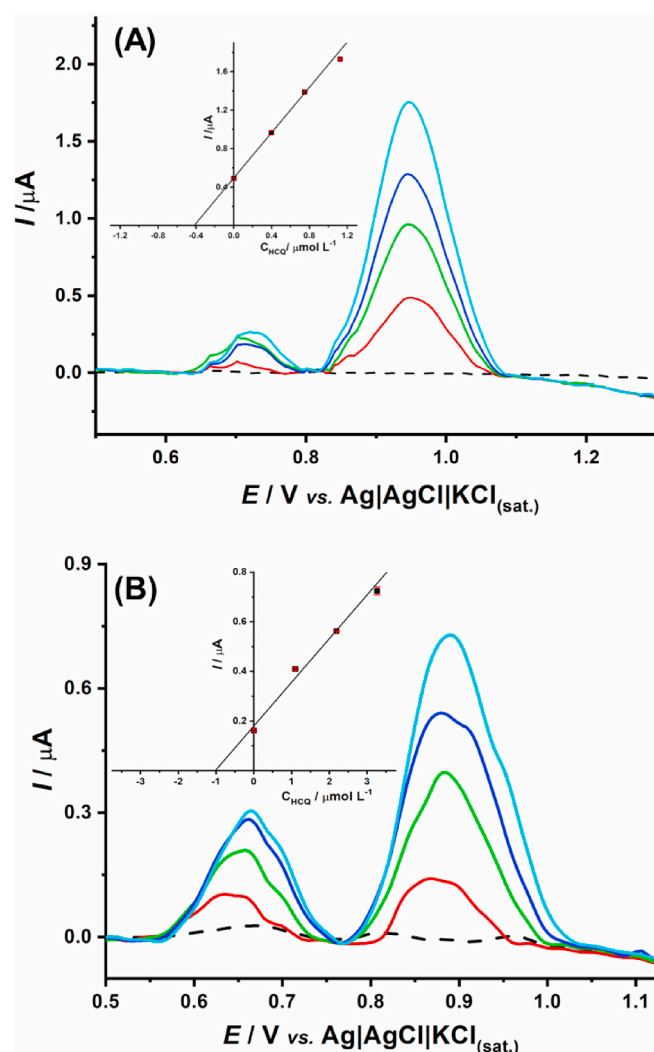
Fig. 7. Baseline-corrected SWV responses for the analysis of **(A)** pharmaceutical tablet (sample A) and **(B)** spiked tap water (sample A) samples diluted in 0.12 mol L^{-1} BR buffer (pH = 9.0) before (supporting electrolyte, dashed line) and after additions of sample (red line) and respective increasing concentrations of HCQ (green, dark blue and light blue lines). Inset: the respective calibration plots. SWV conditions: amplitude = 70 mV; step potential = 4 mV; frequency = 30 s^{-1}. (For interpretation of the references to colour in this figure legend, the reader is referred to the Web version of this article.)

+1.05 V) was investigated for sensing purpose using BR buffer (0.12 mol L^{-1} pH = 9.0) since that higher current peak was achieved when compared to the first HCQ oxidation process.

3.2. HCQ determination in pharmaceutical and tap water samples

The SWV technique was used to demonstrate the applicability of the 3D-printed CB-PLA electrode for the fast and selective detection of HCQ. For this purpose, the parameters of SWV (frequency, amplitude and step potential) were systematically optimized using univariate tests. SWV conditions were selected based on their effect on voltammetric profiles, such as current response, speed of analysis, and the peak shape, using 3.8 µmol L^{-1} HCQ and 0.12 mol L^{-1} BR buffer (pH = 9.0) as the supporting electrolyte (Figs. S2, S3 and S4). The evaluated ranges and respective optimized values are given in Table S2.

After SWV optimized conditions, a calibration plot was constructed upon successive additions of HCQ concentrations using BR buffer (0.12 mol L^{-1}, pH = 9.0) as the supporting electrolyte. A linear response was achieved for standard solutions of HCQ (0.4–7.5 µmol L^{-1}) with a good

Table 1

Results (mean ± SD) obtained for determination of HCQ in pharmaceutical samples by SWV using the 3D-printed CB-PLA electrode and by spectrophotometry (UV region).

Sample	SWV	UV spectrophotometry
Tablet A	367 ± 2 mg	367 ± 6 mg
Tablet B	359 ± 1 mg	364 ± 9 mg

Table 2

Results (mean ± SD) obtained for determination of HCQ in tap water samples by SWV using 3D-printed CB-PLA electrode.

Sample	Spiked/µmol L^{-1}	Found/µmol L^{-1}	Recovery/%
Tap water A	10.0	9.9 ± 0.5	99 ± 5
Tap water B	15.0	16.9 ± 0.1	112 ± 1

linear correlation coefficient (r > 0.994), as noticed in Fig. 6. It was suspected that the short linear range could be related to blockage of the active sites on the electrode surface by the oxidation product of HQ. However, electrochemical measurements were performed using a potassium ferricyanide redox probe before and after the preparation of the calibration plot. Considering that similar voltammetric profiles (peak-to-peak separation and current response) were obtained (Fig. S5), there is no evidence of electrode surface blocking. Therefore, the short linear range can be related to an intrinsic property of the molecule, since the same behavior was already observed when a boron-doped diamond electrode was used [31]. From the calibration plot, the limit of detection (LOD) and sensitivity (slope) were estimated in 0.04 µmol L^{-1} and 0.28 µA L µmol^{-1}, respectively. LOD was calculated based on the IUPAC definition, (LOD = 3σ/s), where s is the slope obtained through the calibration plot from the insert in Fig. 6 and σ is the standard deviation of intercept. Table S3 summarizes the analytical parameters obtained from the data presented in Fig. 6.

The intra-day precision was estimated using the current variation of successive measurements by SWV (n = 10) for 3.4 µmol L^{-1} HCQ (Fig. S6). The RSD value (2.4%) indicates that the method shows good precision and stability. In order to demonstrate the feasibility for the application of 3D-printed CB-PLA sensor, tap water and pharmaceutical samples were analyzed using the standard addition method. For this purpose, tap water was collected and spiked with two HCQ concentration levels (10 and 15 µmol L^{-1}). Next, pharmaceutical and tap water samples were diluted in the supporting electrolyte. Fig. 7 and S7 present SWV responses and the respective calibration plot for pharmaceutical tablet (A) and tap water (B) samples. These results and recovery values obtained in this study are described in Tables 1 and 2.

As can be seen in Table 1, HCQ contents found in the pharmaceutical samples were in agreement with the value provided by the spectrophotometric method. According to the paired *t*-test, the calculated value (0.95) was smaller than the theoretical critical value (12.7, for n = 3), which indicates that the results obtained by both methods are statistically similar (95% confidence level). In addition, satisfactory recovery values (from 99 to 112%) were obtained for tap water samples, which indicated the absence of sample-matrix effects (Table 2).

Subsequently, a selectivity study was performed in the presence of other emerging contaminants, such as azithromycin (AZI), paracetamol (PRT), caffeine (CFN) and acetylsalicylic acid (ACS), using 1.5 µmol L^{-1} HCQ and an HCQ/interferent agent ratio (1:1). As can be seen in Fig. S8, the results indicate an adequate selectivity (variation in HCQ electrochemical response was lower than 12%) in the presence of PRT, CFN, and ACS. However, the current response of HCQ in the presence AZI increased in 40%. According to the literature, AZI has an oxidation process at around +0.9 V (vs. Ag|AgCl|KCl$_{(sat.)}$) which overlaps with HCQ response [62,63]. On the other hand, the first oxidation peak for HCQ can be used for differentiate these species.

The analytical performance of the developed method, such as linear range and LOD, was compared to other electrochemical sensors reported in the literature for HCQ detection (Table 3). As can be observed, many of the sensors use costly materials and requires laborious surface modification steps, which provide an increase in the analysis time. In addition, the analytical performance of the proposed 3D-printed CB-PLA is similar or better than the conventional electrodes. Importantly, the 3D printed CB-PLA electrode is a versatile and inexpensive disposable device with good potential for on-site analysis.

4. Conclusions

This work has demonstrated an electrochemical method for the determination of HCQ in tap water and pharmaceutical samples using 3D-printed CB-PLA electrodes. A substantial increase in the electrochemical response for HCQ was observed after the activation treatment of the 3D-printed electrode surface, leading to similar analytical performance to conventional electrodes. A linear range (0.4–7.5 µmol L^{-1}) and high detectability (LOD = 0.04 µmol L^{-1}) were achieved. The proposed method is simple, low-cost, precise (RSD <2.4%; n = 10) and can be used in laboratories with minimal infrastructure requirements. Moreover, the feasibility of this method was demonstrated through the analysis of tap water and pharmaceutical samples in which showed appropriate accuracy (recovery values between 99 and 112% for tap water samples).

Credit author statement

Mayane S. Carvalho: Conceptualization, Methodology, Data

Table 3

Comparison of the analytical performance obtained using 3D-printed CB/PLA electrode with other electrochemical sensors reported in the literature for HCQ determination.

Electrode	Method	Linear range (µmol L^{-1})	LOD (µmol L^{-1})	Sample	Refs.
SDSMCNTPE	CV	10–40	0.85	Pharmaceutical	[7]
RGO–TiO$_2$/GCE	SWV	0.25–500	0.01	Pharmaceutical	[56]
GCE-PMPDASAM	DPV	10–99	0.004	Serum	[2]
CPE/CNNS	DPV	0.01–7.00	0.00016	Pharmaceutical and urine	[59]
GCE-PMPD SAM	DPV	12–111	0.004	Pharmaceutical; serum	[61]
BDD	SWV	0.1–2.0	0.06	Urine	[31]
MWCNT/CPE	AdSDPV	0.06–100	0.006	Serum	[32]
3D-CB/PLA	SWV	0.4–7.5	0.04	Pharmaceutical; Tap water	This work

SDSMCNTPE: sodium dodecyl sulfate modified carbon nanotube paste electrode; rGO–TiO$_2$/GCE: reduced graphene oxide–TiO$_2$ nanocomposite modified glassy carbon electrode; GCE-PMPDASAM: *N,N*-bis[(E)-(1-pyridyl) methylidene]-1,3-propanediamine self-assembled monolayer on glassy carbon electrode; CGE: coated graphite electrode; CPE/CNNS: carbon paste electrode modified with carbon nitride nanosheets; GCE-PMPD SAM: N,N -bis[(E)-(1-pyridyl) methylidene]-1,3-propanediamine (PMPD) self-assembled monolayer (SAM) on glassy carbon electrode; BDD: boron doped diamond; MWCNT/CPE: carbon paste electrode modified with multi-walled carbon nanotubes; SWV: square wave voltammetry; DPV: differential pulse voltammetry; CV: Cyclic voltammetry; AdSDPV: Adsorptive stripping differential pulse voltammetry.

curation, Investigation, Writing – original draft. Raquel G. Rocha: Data curation, Investigation, Writing – original draft. Lucas V. de Faria: Visualization, Investigation, Supervision, Writing – original draft. Eduardo M. Richter: Supervision, Writing- Reviewing and Editing. Luiza M. F. Dantas: Supervision, Writing- Reviewing and Editing. Iranaldo S. da Silva: Conceptualization, Supervision, Writing- Reviewing and Editing, Funding acquisition. Rodrigo A. A. Muñoz: Conceptualization, Supervision, Writing- Reviewing and Editing, Resources, Funding acquisition, Project administration.

Declaration of competing interest

The authors declare that they have no known competing financial interests or personal relationships that could have appeared to influence the work reported in this paper.

Acknowledgements

Appendix A. Supplementary data

Supplementary data to this article can be found online at https://doi.org/10.1016/j.talanta.2022.123727.

References

[1] K.D. Rainsford, A.L. Parke, M. Clifford-Rashotte, W.F. Kean, Therapy and pharmacological properties of hydroxychloroquine and chloroquine in treatment of systemic lupus erythematosus, rheumatoid arthritis and related diseases, Inflammopharmacology 23 (2015) 231–269, https://doi.org/10.1007/s10787-015-0239-y.

[2] A. Khoobi, S.M. Ghoreishi, M. Behpour, M. Shaterian, M. Salavati-Niasari, Design and evaluation of a highly sensitive nanostructure-based surface modification of glassy carbon electrode for electrochemical studies of hydroxychloroquine in the presence of acetaminophen, Colloids Surf. B Biointerfaces 123 (2014) 648–656, https://doi.org/10.1016/j.colsurfb.2014.10.002.

[3] D.M. Stevens, R.M. Crist, S.T. Stern, Nanomedicine reformulation of chloroquine and hydroxychloroquine, Molecules 26 (2021) 175, https://doi.org/10.3390/molecules26010175.

[4] I. Ben-Zvi, S. Kivity, P. Langevitz, Y. Shoenfeld, Hydroxychloroquine: from malaria to autoimmunity, Clin. Rev. Allergy Immunol. 42 (2012) 145–153, https://doi.org/10.1007/s12016-010-8243-x.

[5] P. Bansal, A. Goyal, A. Cusick, S. Lahan, H.S. Dhaliwal, P. Bhyan, P.B. Bhattad, F. Aslam, S. Ranka, T. Dalia, L. Chhabra, D. Sanghavi, B. Sonani, J.M. Davis, Hydroxychloroquine: a comprehensive review and its controversial role in coronavirus disease 2019, Ann. Med. 53 (2021) 117–134, https://doi.org/10.1080/07853890.2020.1839959.

[6] C. Chatre, F. Roubille, H. Vernhet, C. Jorgensen, Y.M. Pers, Cardiac complications attributed to chloroquine and hydroxychloroquine: a systematic review of the literature, Drug Saf. 41 (2018) 919–931, https://doi.org/10.1007/s40264-018-0689-4.

[7] P.A. Pushpanjali, J.G. Manjunatha, N. Hareesha, T. Girish, A.A. Al-Kahtani, A. M. Tighezza, N. Ataollahi, Electrocatalytic determination of hydroxychloroquine using sodium dodecyl sulphate modified carbon nanotube paste electrode, Top. Catal. (2022) 1–9, https://doi.org/10.1007/s11244-022-01568-8.

[8] FDA, Emergency Use Authorization of Medical Products and Related Authorities, FDA, 2017.

[9] A. Cortegiani, G. Ingoglia, M. Ippolito, A. Giarratano, S. Einav, A systematic review on the efficacy and safety of chloroquine for the treatment of COVID-19, J. Crit. Care 57 (2020) 279–283, https://doi.org/10.1016/j.jcrc.2020.03.005.

[10] K. Kaur, S. Kaushal, I. Kaushal, Therapeutic status of hydroxychloroquine in COVID-19: a review, J. Anaesthesiol. Clin. Pharmacol. 36 (2020) S160–S165, https://doi.org/10.4103/joacp.JOACP_313_20.

[11] A.V. Hernandez, M.T. Phan, J. Rocco, V. Pasupuleti, J.J. Barboza, A. Piscoya, Y. M. Roman, C.M. White, Efficacy and safety of hydroxychloroquine for hospitalized

[12] S. Satarker, T. Ahuja, M. Banerjee, V.B. E, S. Dogra, T. Agarwal, M. Nampoothiri, Hydroxychloroquine in COVID-19: potential mechanism of action against SARS-CoV-2, CurrenCurr Pharmacol Rep.t Pharmacology Reports 6 (2020) 203–211, https://doi.org/10.1007/s40495-020-00231-8.

[13] X. Yao, F. Ye, M. Zhang, C. Cui, B. Huang, P. Niu, X. Liu, L. Zhao, E. Dong, C. Song, S. Zhan, R. Lu, H. Li, W. Tan, D. Liu, In vitro antiviral activity and projection of optimized dosing design of hydroxychloroquine for the treatment of severe acute respiratory syndrome coronavirus 2 (SARS-CoV-2), Clin. Infect. Dis. 71 (2020) 732–739, https://doi.org/10.1093/cid/ciaa237.

[14] E. Chorin, L. Wadhwani, S. Magnani, M. Dai, E. Shulman, C. Nadeau-Routhier, R. Knotts, R. Bar-Cohen, E. Kogan, C. Barbhaiya, A. Aizer, D. Holmes, S. Bernstein, M. Spinelli, D.S. Park, C. Stefano, L.A. Chinitz, L. Jankelson, QT interval prolongation and torsade de pointes in patients with COVID-19 treated with hydroxychloroquine/azithromycin, Heart Rhythm 17 (2020) 1425–1433, https://doi.org/10.1016/j.hrthm.2020.05.014.

[15] E.S. Rosenberg, E.M. Dufort, T. Udo, L.A. Wilberschied, J. Kumar, J. Tesoriero, P. Weinberg, J. Kirkwood, A. Muse, J. Dehovitz, D.S. Blog, B. Hutton, D. R. Holtgrave, H.A. Zucker, Association of treatment with hydroxychloroquine or azithromycin with in-hospital mortality in patients with COVID-19 in New York state, JAMA, J. Am. Med. Assoc. 323 (2020) 2493–2502, https://doi.org/10.1001/jama.2020.8630.

[16] C. Doyno, D.M. Sobieraj, W.L. Baker, Toxicity of chloroquine and hydroxychloroquine following therapeutic use or overdose, Clin. Toxicol. (2020) 12–23, https://doi.org/10.1080/15563650.2020.1817479.

[17] D.R. Boulware, M.F. Pullen, A.S. Bangdiwala, K.A. Pastick, S.M. Lofgren, E. C. Okafor, C.P. Skipper, A.A. Nascene, M.R. Nicol, M. Abassi, N.W. Engen, M. P. Cheng, D. LaBar, S.A. Lother, L.J. MacKenzie, G. Drobot, N. Marten, R. Zarychanski, L.E. Kelly, I.S. Schwartz, E.G. McDonald, R. Rajasingham, T.C. Lee, K.H. Hullsiek, A randomized trial of hydroxychloroquine as postexposure prophylaxis for covid-19, N. Engl. J. Med. 383 (2020) 517–525, https://doi.org/10.1056/nejmoa2016638.

[18] P. Maisonnasse, J. Guedj, V. Contreras, S. Behillil, C. Solas, R. Marlin, T. Naninck, A. Pizzorno, J. Lemaitre, A. Gonçalves, N. Kahlaoui, O. Terrier, R.H.T. Fang, V. Enouf, N. Dereuddre-Bosquet, A. Brisebarre, F. Touret, C. Chapon, B. Hoen, B. Lina, M.R. Calatrava, S. van der Werf, X. de Lamballerie, R. le Grand, Hydroxychloroquine use against SARS-CoV-2 infection in non-human primates, Nature 585 (2020) 584–587, https://doi.org/10.1038/s41586-020-2558-4.

[19] S. Das, A.K. Ramachandran, S.R. Birangal, S. Akbar, B. Ahmed, A. Joseph, The controversial therapeutic journey of chloroquine and hydroxychloroquine in the battle against SARS-CoV-2: a comprehensive review, Med Drug Discov. 10 (2021), 100085, https://doi.org/10.1016/j.medidd.2021.100085.

[20] M. Cochin, F. Touret, J.-S. Driouich, G. Moureau, P.-R. Petit, C. Laprie, C. Solas, X. de Lamballerie, A. Nougairède, Hydroxychloroquine and azithromycin used alone or combined are not effective against SARS-CoV-2 ex vivo and in a hamster model, Antivir. Res. 197 (2022), 105212, https://doi.org/10.1016/j.antiviral.2021.105212.

[21] L.R. de M. Ferraz, F.L.A. dos Santos, P. de A. Ferreira, Ricardo Tadeu Lourenço Maia Junior, T.A. Rosa, L. Araújo Rolim, P.J. Rolim-Neto, Clinical, pharmacokinetic and technological aspects of the hydroxychloroquine sulfate, IOSR J. Pharm. 4 (2014) 53–64, https://doi.org/10.9790/3013-04011053064.

[22] A. Shrivastava, Analytical methods for the determination of hydroxychloroquine in various matrices, Int. J. Appl. Pharm. 12 (2020) 55–61, https://doi.org/10.22159/ijap.2020v12i4.34304.

[23] W.M. El-Koussi, N.N. Atia, G.A. Saleh, N. Hammam, Innovative HPTLC method for simultaneous determination of ternary mixture of certain DMARDs in real samples of rheumatoid arthritis patients: an application of quality by design approach, J. Chromatogr., B: Anal. Technol. Biomed. Life Sci. 1124 (2019) 135–145, https://doi.org/10.1016/j.jchromb.2019.05.038.

[24] N. Armstrong, M. Richez, D. Raoult, E. Chabriere, Simultaneous UHPLC-UV analysis of hydroxychloroquine, minocycline and doxycycline from serum samples for the therapeutic drug monitoring of Q fever and Whipple's disease, J. Chromatogr., B: Anal. Technol. Biomed. Life Sci. 1060 (2017) 166–172, https://doi.org/10.1016/j.jchromb.2017.06.011.

[25] S. Singh, N. Sharma, Y.P. Singla, S. Arora, Development and validation of UV-Spectrophotometric method for quantitative estimation of nefopam hydrochloride in polymethacrylate nanospheres, Int. J. Pharm. Pharmaceut. Sci. 8 (2016) 414–419.

[26] M. Soichot, B. Mégarbane, P. Houzé, L. Chevillard, J. Fonsart, F.J. Baud, O. Laprévote, E. Bourgogne, Development, validation and clinical application of a LC-MS/MS method for the simultaneous quantification of hydroxychloroquine and its active metabolites in human whole blood, J. Pharmaceut. Biomed. Anal. 100 (2014) 131–137, https://doi.org/10.1016/j.jpba.2014.07.009.

[27] L.Z. Wang, R.Y.L. Ong, T.M. Chin, W.L. Thuya, S.C. Wan, A.L.A. Wong, S.Y. Chan, P.C. Ho, B.C. Goh, Method development and validation for rapid quantification of hydroxychloroquine in human blood using liquid chromatography-tandem mass spectrometry, J. Pharmaceut. Biomed. Anal. 61 (2012) 86–92, https://doi.org/10.1016/j.jpba.2011.11.034.

[28] A. Shrivastava, Analytical methods for venlafaxine hydrochloride and metabolites determinations in different matrices, Sys. Rev. Pharm. 3 (2012) 42–50, https://doi.org/10.4103/0975-8453.107141.

[29] M.L.P.M. Arguelho, J.F. Andrade, N.R. Stradiotto, Electrochemical study of hydroxychloroquine and its determination in plaquenil by differential pulse voltammetry, J. Pharmaceut. Biomed. Anal. 32 (2003) 269–275, https://doi.org/10.1016/S0731-7085(02)00669-6.

[30] H. Mater Mahnashi, A.M. Mahmoud, A. Saad Alkahtani, M.M. El-Wekil, Simultaneous electrochemical detection of azithromycin and hydroxychloroquine based on VS2 QDs embedded N, S @graphene aerogel/cCNTs 3D nanostructure, Microchem. J. 163 (2021), 105925, https://doi.org/10.1016/j.microc.2021.105925.

[31] P.B. Deroco, F.C. Vicentini, G.G. Oliveira, R.C. Rocha-Filho, O. Fatibello-Filho, Square-wave voltammetric determination of hydroxychloroquine in pharmaceutical and synthetic urine samples using a cathodically pretreated boron-doped diamond electrode, J. Electroanal. Chem. 719 (2014) 19–23, https://doi.org/10.1016/j.jelechem.2014.01.037.

[32] S.M. Ghoreishi, A.M. Attaran, A.M. Amin, A. Khoobi, Multiwall carbon nanotube-modified electrode as a nanosensor for electrochemical studies and stripping voltammetric determination of an antimalarial drug, RSC Adv. 5 (2015) 14407–14415, https://doi.org/10.1039/C4RA16357E.

[33] E. Vaněčková, M. Bouša, Š. Nováková Lachmanová, J. Rathouský, M. Gál, T. Sebechlebská, V. Kolivoška, 3D printed polylactic acid/carbon black electrodes with nearly ideal electrochemical behaviour, J. Electroanal. Chem. 857 (2020), https://doi.org/10.1016/j.jelechem.2019.113745.

[34] V. Katseli, A. Economou, C. Kokkinos, Single-step fabrication of an integrated 3D-printed device for electrochemical sensing applications, Electrochem. Commun. 103 (2019) 100–103, https://doi.org/10.1016/j.elecom.2019.05.008.

[35] L. Fiore, B. de Lellis, V. Mazzaracchio, E. Suprun, R. Massoud, B.M. Goffredo, D. Moscone, F. Arduini, Smartphone-assisted electrochemical sensor for reliable detection of tyrosine in serum, Talanta 237 (2022), 122869, https://doi.org/10.1016/j.talanta.2021.122869.

[36] R.M. Cardoso, C. Kalinke, R.G. Rocha, P.L. dos Santos, D.P. Rocha, P.R. Oliveira, B. C. Janegitz, J.A. Bonacin, E.M. Richter, R.A.A. Munoz, Additive-manufactured (3D-printed) electrochemical sensors: a critical review, Anal. Chim. Acta. 1118 (2020) 73–91, https://doi.org/10.1016/j.aca.2020.03.028.

[37] J. Muñoz, M. Pumera, Accounts in 3D-printed electrochemical sensors: towards monitoring of environmental pollutants, Chemelectrochem 7 (2020) 3404–3413, https://doi.org/10.1002/celc.202000601.

[38] E.M. Richter, D.P. Rocha, R.M. Cardoso, E.M. Keefe, C.W. Foster, R.A.A. Munoz, C. E. Banks, Complete additively manufactured (3D-printed) electrochemical sensing platform, Anal. Chem. 91 (2019) 12844–12851, https://doi.org/10.1021/acs.analchem.9b02573.

[39] J.S. Stefano, C. Kalinke, R.G. da Rocha, D.P. Rocha, V.A.O.P. da Silva, J.A. Bonacin, L. Angnes, E.M. Richter, B.C. Janegitz, R.A.A. Muñoz, Electrochemical (Bio)Sensors enabled by fused deposition modeling-based 3D printing: a guide to selecting designs, printing parameters, and post-treatment protocols, Anal. Chem. 94 (2022) 6417–6429, https://doi.org/10.1021/acs.analchem.1c05523.

[40] L.C. Duarte, T.A. Baldo, H.A. Silva-Neto, F. Figueredo, B.C. Janegitz, W.K.T. Coltro, 3D printing of compact electrochemical cell for sequential analysis of steroid hormones, Sens. Actuators B: Chem. 364 (2022), 131850, https://doi.org/10.1016/j.snb.2022.131850.

[41] C. Tan, M.Z.M. Nasir, A. Ambrosi, M. Pumera, 3D printed electrodes for detection of nitroaromatic explosives and nerve agents, Anal. Chem. 89 (2017) 8995–9001, https://doi.org/10.1021/acs.analchem.7b01614.

[42] E. Vaněčková, M. Bouša, Š. Nováková Lachmanová, J. Rathouský, M. Gál, T. Sebechlebská, V. Kolivoška, 3D printed polylactic acid/carbon black electrodes with nearly ideal electrochemical behaviour, J. Electroanal. Chem. 857 (2020), 113745, https://doi.org/10.1016/j.jelechem.2019.113745.

[43] A.F. João, R.G. Rocha, T.A. Matias, E.M. Richter, J. Flávio S. Petruci, R.A. A. Muñoz, 3D-printing in forensic electrochemistry: atropine determination in beverages using an additively manufactured graphene-polylactic acid electrode, Microchem. J. 167 (2021), 106324, https://doi.org/10.1016/j.microc.2021.106324.

[44] R.M. Cardoso, D.M.H. Mendonça, W.P. Silva, M.N.T. Silva, E. Nossol, R.A.B. da Silva, E.M. Richter, R.A.A. Muñoz, 3D printing for electroanalysis: from multiuse electrochemical cells to sensors, Anal. Chim. Acta. 1033 (2018) 49–57, https://doi.org/10.1016/j.aca.2018.06.021.

[45] R.M. Cardoso, S.V.F. Castro, M.N.T. Silva, A.P. Lima, M.H.P. Santana, E. Nossol, R. A.B. Silva, E.M. Richter, T.R.L.C. Paixão, R.A.A. Muñoz, 3D-printed flexible device combining sampling and detection of explosives, Sens. Actuators B: Chem. 292 (2019) 308–313, https://doi.org/10.1016/j.snb.2019.04.126.

[46] M. Di-Oliveira, R.G. Rocha, L. v de Faria, E.M. Richter, R.A.A. Munoz, Carbon-black integrated polylactic acid electrochemical sensor for chloramphenicol determination in milk and water samples, J. Electrochem. Soc. 169 (2022), 047517, https://doi.org/10.1149/1945-7111/ac6454.

[47] A.F. João, L.v. de Faria, D.L.O. Ramos, R.G. Rocha, E.M. Richter, R.A.A. Muñoz, 3D-printed carbon black/polylactic acid electrochemical sensor combined with

batch injection analysis: a cost-effective and portable tool for naproxen sensing, Microchem. J. 180 (2022), 107565, https://doi.org/10.1016/j.microc.2022.107565.

[48] N.I.G. Inoque, A.F. João, L.v. de Faria, R.A.A. Muñoz, Electrochemical determination of several biofuel antioxidants in biodiesel and biokerosene using polylactic acid loaded with carbon black within 3D-printed devices, Microchim. Acta. 189 (2022) 57, https://doi.org/10.1007/s00604-021-05152-x.

[49] T.P. Lisboa, G.F. Alves, L.V. de Faria, C.C. de Souza, M.A.C. Matos, R.C. Matos, 3D-printed electrode an affordable sensor for sulfanilamide monitoring in breast milk, synthetic urine, and pharmaceutical formulation samples, Talanta 247 (2022), 123610, https://doi.org/10.1016/j.talanta.2022.123610.

[50] V.N. Ataide, D.P. Rocha, A. de Siervo, T.R.L.C. Paixão, R.A.A. Muñoz, L. Angnes, Additively manufactured carbon/black-integrated polylactic acid 3Dprintedsensor for simultaneous quantification of uric acid and zinc in sweat, Microchim. Acta. 188 (2021) 388, https://doi.org/10.1007/s00604-021-05007-5.

[51] H.A. Silva-Neto, A.A. Dias, W.K.T. Coltro, 3D-printed electrochemical platform with multi-purpose carbon black sensing electrodes, Microchim. Acta. 189 (2022) 235, https://doi.org/10.1007/s00604-022-05323-4.

[52] E. Vaněčková, M. Bouša, V. Shestivska, J. Kubišta, P. Moreno-García, P. Broekmann, M. Rahaman, M. Zlámal, J. Heyda, M. Bernauer, T. Sebechlebská, V. Kolivoška, Electrochemical reduction of carbon dioxide on 3D printed electrodes, Chemelectrochem 8 (2021) 2137–2149, https://doi.org/10.1002/celc.202100261.

[53] P.E.M. 1323, British Pharmacopoeia 2009, vol. 3, 2009.

[54] L.R. M Ferraz, F.L. A Santos, P.A. Ferreira, R.T. L Maia-Junior, T.A. Rosa, S.P. M Costa, C.M. Melo, L.A. Rolim, P.J. Rolim-Neto, Quality by design in the development and validation of analytical method by ultraviolet-visible spectrophotometry for quantification of hydroxychloroquine sulfate, Int. J. Pharmaceut. Sci. Res. 5 (2014) 4666, https://doi.org/10.13040/IJPSR.0975-8232.5(11).4666-76.

[55] R.G. Rocha, J.S. Ribeiro, M.H.P. Santana, E.M. Richter, R.A.A. Muñoz, 3D-printing for forensic chemistry: voltammetric determination of cocaine on additively manufactured graphene–polylactic acid electrodes, Anal. Methods. 13 (2021) 1788–1794, https://doi.org/10.1039/D1AY00181G.

[56] H. Zhang, L. Cheng, H. Shang, W. Zhang, A. Zhang, A novel electrochemical sensor based on reduced graphene oxide–TiO2 nanocomposites with high selectivity for the determination of hydroxychloroquine, Russ. J. Electrochem. 57 (2021) 872–884.

[57] D.P. Rocha, A.L. Squissato, S.M. da Silva, E.M. Richter, R.A.A. Munoz, Improved electrochemical detection of metals in biological samples using 3D-printed electrode: chemical/electrochemical treatment exposes carbon-black conductive sites, Electrochim. Acta 335 (2020) 1–11, https://doi.org/10.1016/j.electacta.2020.135688.

[58] R.M. Cardoso, P.R.L. Silva, A.P. Lima, D.P. Rocha, T.C. Oliveira, T.M. do Prado, E. L. Fava, O. Fatibello-Filho, E.M. Richter, R.A.A. Muñoz, 3D-Printed graphene/polylactic acid electrode for bioanalysis: biosensing of glucose and simultaneous determination of uric acid and nitrite in biological fluids, Sensor. Actuator. B Chem. 307 (2020) 127621, https://doi.org/10.1016/j.snb.2019.127621.

[59] J. Oliveira S. Silva, M.V.S. Sant'Anna, A. Gevaerd, J.B.S. Lima, M.D.S. Monteiro, S. W.M.M. Carvalho, E. Midori Sussuchi, A novel carbon nitride nanosheets-based electrochemical sensor for determination of hydroxychloroquine in pharmaceutical formulation and synthetic urine samples, Electroanalysis 33 (2021) 2152–2160, https://doi.org/10.1002/elan.202100170.

[60] E. Laviron, A. Vallat, R. Meunier-Prest, The reduction mechanism of aromatic nitro compounds in aqueous medium: Part V. The reduction of nitrosobenzene between pH 0.4 and 13, J. Electroanal. Chem. 379 (1994) 427–435, https://doi.org/10.1016/0022-0728(94)87167-1.

[61] S.M. Ghoreishi, M. Behpour, A. Khoobi, M. Salavati-Niasari, Electrochemical study of a self-assembled monolayer of N,N′-bis[(E)-(1-pyridyl) methylidene]-1,3-propanediamine formed on glassy carbon electrode: preparation, characterization and application, Anal. Methods. 5 (2013) 6727–6733, https://doi.org/10.1039/C3AY41480A.

[62] W.B. Veloso, A.T. de F.O. Almeida, L.K. Ribeiro, M. de Assis, E. Longo, M.A. S. Garcia, A.A. Tanaka, I. Santos da Silva, L.M.F. Dantas, Rapid and sensitivity determination of macrolides antibiotics using disposable electrochemical sensor based on Super P carbon black and chitosan composite, Microchem. J. 172 (2022), https://doi.org/10.1016/j.microc.2021.106939.

[63] J.Y. Peng, C.T. Hou, X.X. Liu, H.B. Li, X.Y. Hu, Electrochemical behavior of azithromycin at graphene and ionic liquid composite film modified electrode, Talanta 86 (2011) 227–232, https://doi.org/10.1016/j.talanta.2011.09.005.